ISSN 1674-1056
http://cpb.iphy.ac.cn
http://iopscience.iop.org/cpb
中国物理 B
Chinese Physics
中国物理
Chinese Physics B

Photon-in/photon-out endstation for studies of energy materials at beamline 02B02 of Shanghai Synchrotron Radiation Facility

Guoxi Ren(任国玺)[1,2,3], Nian Zhang(张念)[1,2], Xuefei Feng(冯雪飞)[1,2], Hui Zhang(章辉)[1,2], Pengfei Yu(于鹏飞)[1,2], Shun Zheng(郑顺)[1,2,3], Deng Zhou(周橙)[1,2,3], Zongwang Tian(田宗旺)[1,2,4], Xiaosong Liu(刘啸嵩)[1,2,4]

Citation: Chin. Phys. B . 2020, 29(1): 016101 . **doi:** 10.1088/1674-1056/ab5d04
Journal homepage: http://cpb.iphy.ac.cn; http://iopscience.iop.org/cpb

What follows is a list of articles you may be interested in

Low temperature *Pmmm* and *C2/m* phases in $Sr_2CuO_{3+\delta}$ high temperature superconductor

Hai-Bo Wang(王海波), Zhen-Lin Luo(罗震林), Yuan-Jun Yang(杨远俊), Qing-Qing Liu(刘清青), Si-Xia Hu(胡思侠), Meng-Meng Yang(杨蒙蒙), Chang-Qing Jin(靳常青), Chen Gao(高琛)

Chin. Phys. B . 2019, 28(5): 056103 . **doi:** 10.1088/1674-1056/28/5/056103

Extended x-ray absorption fine structure study of $MnFeP_{0.56}Si_{0.44}$ compound

Li Ying-Jie, Haschaolu W, Wurentuya, Song Zhi-Qiang, Ou Zhi-Qiang, Tegus O, Nakai Ikuo

Chin. Phys. B . 2015, 24(8): 086101 . **doi:** 10.1088/1674-1056/24/8/086101

SPECIAL TOPIC — Advanced calculation & characterization of energy storage materials & devices at multiple scale

Photon-in/photon-out endstation for studies of energy materials at beamline 02B02 of Shanghai Synchrotron Radiation Facility*

Guoxi Ren(任国玺)[1,2,3,†], Nian Zhang(张念)[1,2,†], Xuefei Feng(冯雪飞)[1,2,§], Hui Zhang(章辉)[1,2], Pengfei Yu(于鹏飞)[1,2], Shun Zheng(郑顺)[1,2,3], Deng Zhou(周橙)[1,2,3], Zongwang Tian(田宗旺)[1,2,4], and Xiaosong Liu(刘啸嵩)[1,2,4,‡]

[1] *State Key Laboratory of Functional Materials for Informatics, Shanghai Institute of Microsystem and Information Technology, Chinese Academy of Sciences, Shanghai* 200050, *China*

[2] *CAS Center for Excellence in Superconducting Electronics (CENSE), Chinese Academy of Sciences, Shanghai* 200050, *China*

[3] *University of Chinese Academy of Sciences, Beijing* 100049, *China*

[4] *School of Physical Science and Technology, Shanghai Tech University, Shanghai* 201210, *China*

(Received 30 October 2019; revised manuscript received 15 November 2019; accepted manuscript online 29 November 2019)

A new photon-in/photon-out endstation at beamline 02B02 of the Shanghai Synchrotron Radiation Facility for studying the electronic structure of energy materials has been constructed and fully opened to users. The endstation has the capability to perform soft x-ray absorption spectroscopy in total electron yield and total fluorescence yield modes simultaneously. The photon energy ranges from 40 eV to 2000 eV covering the *K*-edge of most low *Z*-elements and the *L*-edge of 3d transition-metals. The new self-designed channeltron detector allows us to achieve good fluorescence signals at the low photon flux. In addition, we synchronously collect the signals of a standard reference sample and a gold mesh on the upstream to calibrate the photon energy and monitor the beam fluctuation, respectively. In order to cross the pressure gap, *in situ* gas and liquid cells for soft x-ray absorption spectroscopy are developed to study the samples under realistic working conditions.

Keywords: soft x-ray absorption, energy materials, photon-in/photon-out, *in situ* cell

PACS: 61.05.cj, 07.85.Qe, 88.80.–q **DOI:** 10.1088/1674-1056/ab5d04

1. Introduction

Sustainable development of energy and environment has become one of the most critical global challenges in the 21st century. The prosperity of electric vehicles and portable devices significantly stimulates the research and development of novel energy storage materials with high capacity and safety.[1,2] Meanwhile, the discovery of new cost-effective and high-active catalysts for energy conversion and storage is essential to renewable energy production.[3,4] Physical and chemical processes happening at the material surfaces and interfaces play an important role in both energy storage materials and catalysts, such as adsorption, desorption, ion/electron exchange, surface re-construction, and heterogeneous catalysis. Therefore, there is an urgent demand to develop multiscale characterization to investigate the surface and interfacial reactions of energy materials. Under this demand, many large research programs and facilities have been established. Among them, the third-generation synchrotron radiation facilities are the representative, such as the Shanghai Synchrotron Radiation Facility (SSRF) that has become a key platform for energy material research.[5–8]

The high-brightness and broad-spectrum x-ray generated by synchrotron facilities expands the multiscale characterization toolbox. Among various techniques, synchrotron-based x-ray absorption spectroscopy (XAS) is a powerful tool to study compositions and chemical states of elements in materials. During XAS experiments, the absorption of photons results in the excitation of a core electron to an unoccupied state above the Fermi level on the basis of selection rules. Thus, XAS provides the detailed information of the unoccupied electronic structure, such as spin states, ligand structure, and hybridization, which are the key factors to regulate the fundamental properties and practical performances of materials. For studying catalytic and energy materials, soft x-ray absorption spectroscopy (sXAS) has its own unique advantages. Firstly, sXAS is direct and sensitive in studying the electronic structure of 3d transition-metals (TMs), which are important for energy materials, such as $LiCoO_2$,[9] $Li(NiCoMn)_{1/3}O_2$,[10] $LiNi_{0.5}Mn_{1.5}O_4$,[11] and catalytic materials $SrCoO_3$ and CoNC.[12] Secondly, soft x-ray also accesses the excitation energy range of most low-*Z* elements,

*Project supported by the National Natural Science Foundation of China (Grant No. 11227902) as part of NSFC ME2 beamline project, Science and Technology Commission of Shanghai Municipality, China (Grant No. 14520722100), and the National Natural Science Foundation of China (Grant Nos. 11905283 and U1632269).

†These authors contributed equally to this work.

‡Corresponding author. E-mail: xliu3@mail.sim.ac.cn

§Present address: Advanced Light Source, Lawrence Berkeley National Laboratory, Berkeley, California 94720, USA

© 2020 Chinese Physical Society and IOP Publishing Ltd

such as Li, C, N, O, F, Na, Si, which are the main compositions of energy storage materials. Finally, sXAS data can be collected by the total electron yield (TEY) signals with probing depth less than 10 nm as well as by the total fluorescence yield (TFY) signals that are bulk sensitive with the penetration depth of typically several hundreds of nanometers. The different probe depths play a significant role in studying the surface catalysis, the coating materials, and the solid electrolyte interface (SEI) layer.[9,13,14] In addition, unlike other traditional laboratory experimental methods, the sXAS mainly focuses on the characterization of electronic structure at the surface ranging from 5–100 nm, which fills the blank of conventional means in multiscale characterization. By combining other characterization methods with sXAS, we can establish the structure–activity relationship between the electronic structure and actual properties, which provides guidance for research of high performance electrochemical energy storage materials. For instance, by combining morphology characterization with *in situ* sXAS, Liu *et al.* revealed the charge dynamics in battery electrodes that are regulated by charge transport, mesoscale morphology, and phase transformation.[15] By combining DFT simulations with sXAS, Rao *et al.* identified in amorphous $Ti_{0.4}Sb_2Te_3$ that the titanium atoms preferably maintain the octahedral configuration.[16] By combining operando XAFS with *ex situ* sXAS, Zhang *et al.* unraveled that the appearance of Co^{4+} and oxidized oxygen ions in $Li_2Co_2O_4$ is tightly accompanied by the surface reconstruction.[17]

Nowadays, hard x-ray (> 5 keV) absorption spectroscopy instruments have been maturely constructed in China, such as beamline 14W1 in SSRF and beamline 1W1B in Beijing Synchrotron Radiation Facility (BSRF), which have been widely used in probing both physical and chemical properties of energy and catalytic materials.[5,18–22] However, sXAS has not been fully developed and utilized for energy materials, particularly for those materials under *in situ* and/or *operando* conditions. This is mainly due to the strict vacuum conditions, lacking powerful detector and applicable *in situ* cells. Thus, it is a sufficient need to construct a high-performance soft x-ray absorption spectroscopy endstation at domestic synchrotron radiation facility for the *ex/in situ* studies of energy and catalytic materials.

Here, we will introduce a new photon-in/photon-out (PIPO) endstation for soft x-ray absorption spectroscopy constructed at beamline 02B02 of SSRF. The sXAS data can be collected by TEY and TFY modes simultaneously in an ultrahigh vacuum chamber. A series of designs, including the beam delivery system, sample holders, the sample preparation system, and *in situ* cells, are focusing on the characterization of energy and catalytic materials. This endstation provides the opportunities to push the sXAS capability to study the materials under *in situ* and/or *operando* conditions. A detailed description of the platform and its performance are given below.

2. System overview

The PIPO endstation is connected to the beamline 02B02 of SSRF. The new bending magnet beamline delivers soft x-ray photons with photon flux around 1×10^{11} photons/s @$E/\Delta E = 3700$ and a tightly focused beam spot size (~ 150 μm$\times 50$ μm) at the sample. To obtain high energy resolution and greater grating diffraction efficiency, three gratings are optimized for varying energy ranges. Gratings with line densities of 400 lines/mm , 800 lines/mm, and 1100 lines//mm cover the energy ranges of 40–600 eV, 200–1600 eV, and 200–2000 eV, respectively. The maximum energy resolution can reach up to 13000 at 250 eV.[23,24] The energy range contains the *K*-edges of C, N, O, F, Na, Mg, Al, Si and the *L*-edges of P, S, Cl, K, Ca, 3d transition-metals, which are important for most energy and catalytic materials.

The PIPO endstation is tailored to provide a powerful sXAS method to study energy and catalytic materials. By fully considering the beamline specifics and the requirements of users, the endstation is self-designed into three main parts: the beam delivery system, the analysis chamber, and the preparation chamber. In addition, *in situ* cells are designed for separate connection onto the main chamber. The layout of the whole endstation is shown in Fig. 1(a). The detailed descriptions of these parts are given below.

2.1. The beam delivery system

The beam delivery system located between the last focusing mirror and the analysis chamber, which consists of four main parts including a standard sample chamber, a double knife slit chamber, a gold mesh chamber, and a pinhole gate valve. As the photon energy and flux change with the operating state of the storage ring in real-time, the standard samples and a gold mesh are used to demarcate the real photon energy and flux. The design of the standard sample chamber is shown in Fig. 1(b). Simultaneous measurement of the real sample and standard sample can be achieved by rotating the standard sample, which blocks $\sim 20\%$ intensity of the whole light on it, while the other 80% still on the real sample. The *K*-edges of O and C are calibrated by standard sample $SrTiO_3$ and SiC single crystals. The *L*-edges of Ti, Mn, Co, Fe, Ni are calibrated by $SrTiO_3$, MnO, CoO, FeO, and NiO single crystals. The fluctuation of the incident x-ray photon flux in real-time is monitored by the drain current of a gold mesh (Precision-eforming M49 gold mesh, wire line width 13 μm, opening width 203 μm, 83% transmittance) (shown in Fig. 1(c)). An evaporator crucible installed below the gold mesh can evaporate Au to maintain the surface cleanliness of the gold mesh. The double knife slit chamber is used to remove stray light

for improving the energy resolution, which is between the standard sample chamber and the gold mesh chamber. Fluorescent powders are painted on both knives to determine the beam position. The pinhole gate valve locates at the end of the beam delivery system shown in Fig. 1(d). A silicon nitride (Si_3N_4) window (1 mm $\times$1 mm, thickness 100 nm) is mounted on the hole, which allows 70% transmittance at photon energy 500 eV. The valve is designed to protect the beamline for doing *in situ*/*operando* experiments with gas and liquid cells. When we do normal XAS experiments, the valve is outside the beam path.

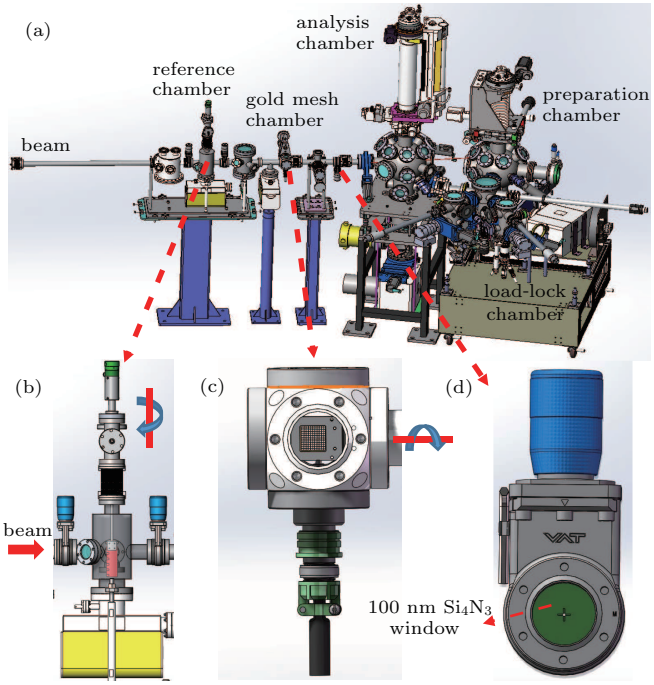


Fig. 1. (a) The layout of the whole endstation. The design of (b) the standard sample chamber, (c) the gold mesh chamber, and (d) the pinhole gate valve.

2.2. The analysis chamber

The analysis chamber is equipped with a four-axis manipulator system (shown in Fig. 2(a)) which consists of a home-built sample stage, an *XYZ* stage (Vacgen, Omiax), and a differentially-pumped rotary platform (Thermionics, RNN-400). The sample stage (shown in Fig. 2(c)) contains two parts, including a low-temperature system (70–300 K) and a high-temperature system (300–600 K). For the low-temperature system, the Janis ST-400 ultra-high vacuum (UHV) cryostat and the sample stage are connected through a 10 mm thickness sapphire plate, which is used as the insulation layer. Both sides of the sapphire plate are pasted with indium to improve the interfacial contact and thermal conductance ability. The K-type thermocouple may create current signals in working conditions, causing a strong impact on the TEY measurement. Thus, a diode thermometer (70–700 K) is installed on the backboard of the sample stage for the temperature measurement in TEY experiment. The high-temperature stage is hung under the low-temperature stage through thermal insulation materials. The thermal insulation materials can protect the diode thermometer in Janis cryostat as it only bears 473 K. The heating module is directly integrated on the backboard of the sample stage.

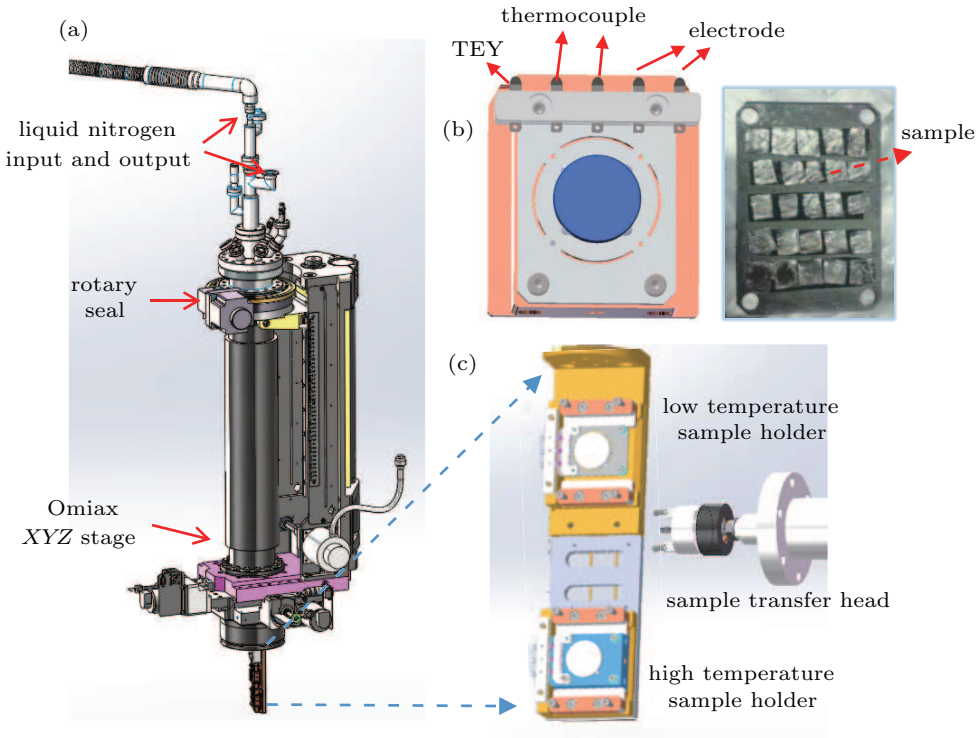


Fig. 2. (a) The layout of the home-built manipulator. (b) The design of the sample holder. (c) The design of the sample stage and transfer arm.

Unlike ambient pressure photoelectron spectroscopy (APPES) and angle resolved photoemission spectroscopy (ARPES) mainly focusing on a single sample, the users of sXAS usually need to measure a serious of samples, including various standard samples. In order to save injection time in the load-lock chamber and do *in situ* battery experiments, the sample holder is designed big enough for coin cell or nearly 20 samples with a 2 mm×2 mm size (shown in Fig. 2(b)). Five thimble spring laminations are reserved in both high-temperature and low-temperature sample holders. Two of them are used as electrodes applying a voltage on the sample. Another two are the K-type thermal couple, which is used for the temperature correction of the diode thermometer on the background of the sample stage. The last one is designed for TEY measurement when the sample needs to be insulated from the sample stage.

The sample in the analysis chamber can be measured by TEY and TFY modes simultaneously. For the XAS measurement in TEY mode, the background current is the key factor to get a good spectrum, because it not only influences the ratio of signal to noise but also determines the minimum amount of elements that can be detected. Thus, decreasing the background current is extremely important. In the analysis chamber, highly shielded coaxial cable and single pin coaxial feedthrough are used. The shielding layer of the cable is connected to the ground through the shell of a self-designed studdle. Meanwhile, out of the chamber, the Femto collector is fastened next to the single pin coaxial feedthrough. So a very short highly shielded BNC cable is used for the transmission of the weak current signals to the Femto collector. Finally, the voltage signals between −10 V and 10 V transformed by the Femto collector are recorded by a NI acquisition card (shown in Fig. 3(a)). With these efforts, the jitter of the background current can be decreased to lower than 0.01 pA. For the sXAS measurement in TFY mode, the beam photon flux is the main challenge, because beamline 02B is a bending magnet beamline with photon flux just around 1×10^{11} photons/s $@E/\Delta E = 3700$, and the fluorescence yield is only about 1% in the soft x-ray region. Thus a Sjuts channel electron multiplier (CEM) is used for acquiring the fluorescence signals. The Sjuts CEM is chosen for outstanding features including compact size, high collection efficiency, and special design for easy mounting. In addition, the Sjuts CEM is not sensitive to visible light, which eliminates possible interference with lamplight. The schematic diagram of the TFY detector is shown in Fig. 3(b). The double-layer gold mesh (one with +50 V voltage and the other with −2000 V) in front of the CEM is used for filtering out photoelectrons and positive ions. By using a linear actuator before the electrical feedthrough, the distance between the double-layer gold mesh and the sample can be adjusted from 3 cm to 11 cm. The fluorescence signal increases with the distance decreasing. However, a distortion of TEY wave mode compared with normal TEY spectrum is observed when the distance decreasing to 3 cm. Thus, we choose 4 cm as the optimize distance, which can not only pick up the maximum fluorescence signals but also avoid high voltage influences on the TEY signals. After a series of special designs, the channeltron detector allows us to achieve good fluorescence signals even at the low photon flux.

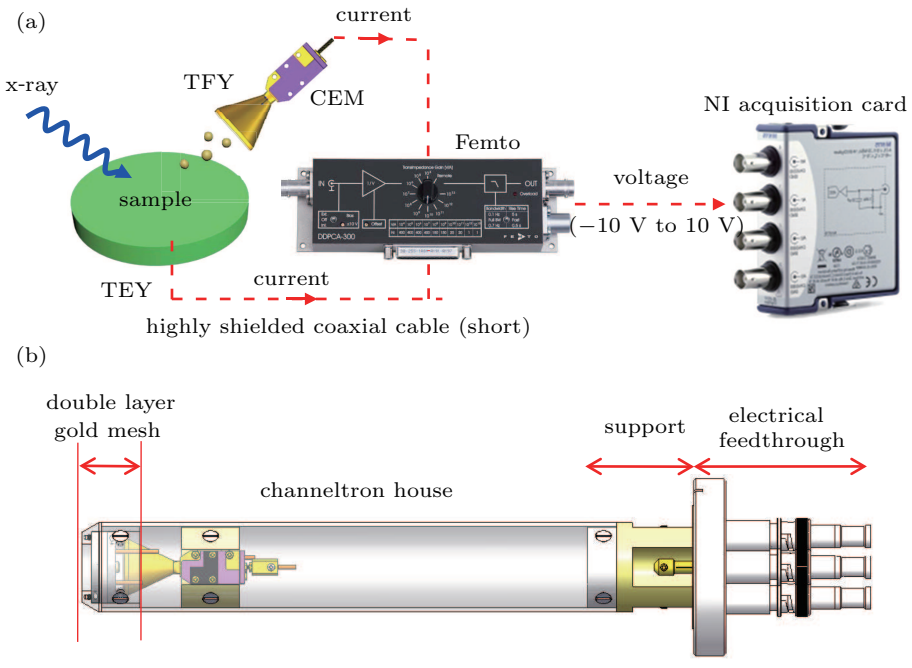


Fig. 3. (a) The schematic depiction of data acquisition for TEY and TFY measurements. (b) The design of the TFY detector.

2.3. The preparation chamber

A lot of energy and catalytic materials are air-sensitive, thus a special glove box is designed on the load-lock chamber to avoid air exposure of the samples. For the samples needing preprocessing, we provide Ar ion etching and vacuum annealing in the preparation chamber. Three individual evaporators (FERMION Instruments Co., Ltd) are also installed on the preparation chamber for the sample growth. The growth rates can be monitored by a quartz crystal microbalance. For single-crystal samples, low energy electron diffraction (OCI, BDL600IR-3GR) is equipped to characterize the surface conditions after preprocessing.

2.4. The *in situ* cells

In order to cross the pressure gap and achieve soft x-ray measurements of samples under real working conditions, the *in situ* cell needs to be used. Different types of *in situ* cells for sXAS measurements have been designed and fabricated at foreign synchrotron facilities, which are used for studying energy materials and catalytic reactions in real working conditions.[25–28] However, no such cells have been successfully used in sXAS endstation at domestic synchrotron facilities. So we design a new high-temperature gas cell, which can collect TEY and TFY signals of samples under ambient pressure conditions. Figure 4(a) shows the design of the high-temperature gas cell at beamline 02B02. The cell is horizontally connected to the analysis chamber through an *XYZ* manipulator. The cell is manufactured by special stainless steel that is chosen for its chemical inertness. Ultrathin 100 nm Si_3N_4 (1 mm×1 mm in size) membrane as a window can be penetrated by x-ray and used for sealing the gas, which makes it fully compatible with the ultrahigh vacuum requirements of the beamline and spectroscopy endstation. The cross-section of the cell is shown in Fig. 4(c). In order to reduce the attenuation of gas for x-ray and fluorescent photons, the gap between the window and the sample is set to be 200 μm. The substrate is coated with gold to increase electrical conductivity for TEY measurement. Two polytetrafluoroethylene (PTFE) pipes allow us to feed the cell volume with different types of gases. The pressure of the cell can reach up to 1 bar. A ceramic heater inside the cell can heat the sample to 600 K. A pinhole gate valve is designed in front of the analysis chamber to protect the beamline. Except for the gas cell, the liquid cell is under construction and may be completed in the next year. As the *in situ* experiment is very dependent on the photon flux of the soft x-ray beamline, the gas cell is still in optimizing signals and may open to the public in the near future.

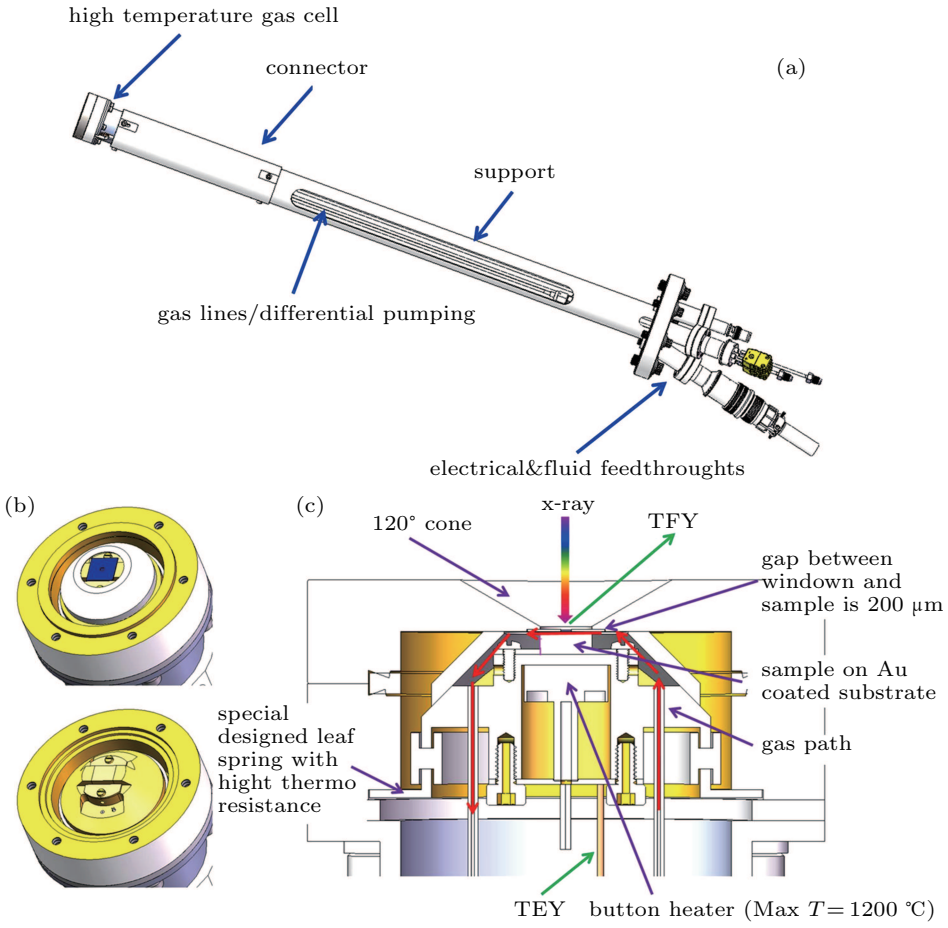


Fig. 4. (a) The design for the high-temperature gas cell. (b) The head of the cell and the sample holder. (c) Cross-section sketch of the gas cell.

3. Results and discussion

The beamline 02B is a bending-magnet beamline. The photon fluxes of the 400 lines/mm, 800 lines/mm, and 1100 lines/mm gratings[23] are shown in Fig. 5(a). The spot size on the PIPO sample is measured to be 150 μm×46 μm[23] (shown in Fig. 5(b)). The parameters mean that the maximum flux is 8×10^{10} photons/s (0.1% bandwidth) at O *K*-edge and 3×10^{10} photons/s (0.1% bandwidth) at transition metal (TM) *L*-edge. Under this photon flux, we detect the current signals about 35 pA on the gold mesh and about 100 pA on the real sample ($SrTiO_3$ single crystal) in the analysis chamber at photon energy 530 eV. Benefitting from our effort to decreasing the jitter of the background currents to lower than 0.01 pA, we can turn down the slits to achieving a high resolution. A high signal to noise ratio TEY spectrum can be measured with only 1 pA current signals on the sample. Figures 5(c)–5(e) show some high-resolution TEY spectra measured at the PIPO endstation. Four clear features can be observed at Co *L*-edge of CoO and a complex O *K* edge spectrum of $SrTiO_3$ is detected. Among the energy materials, sodium battery is one of the most common systems. We detect high quality Na *K*-edge sXAS spectrum using Na_2SO_4 powder at around 1072 eV, which is difficult to realize in other sXAS endstations at home.

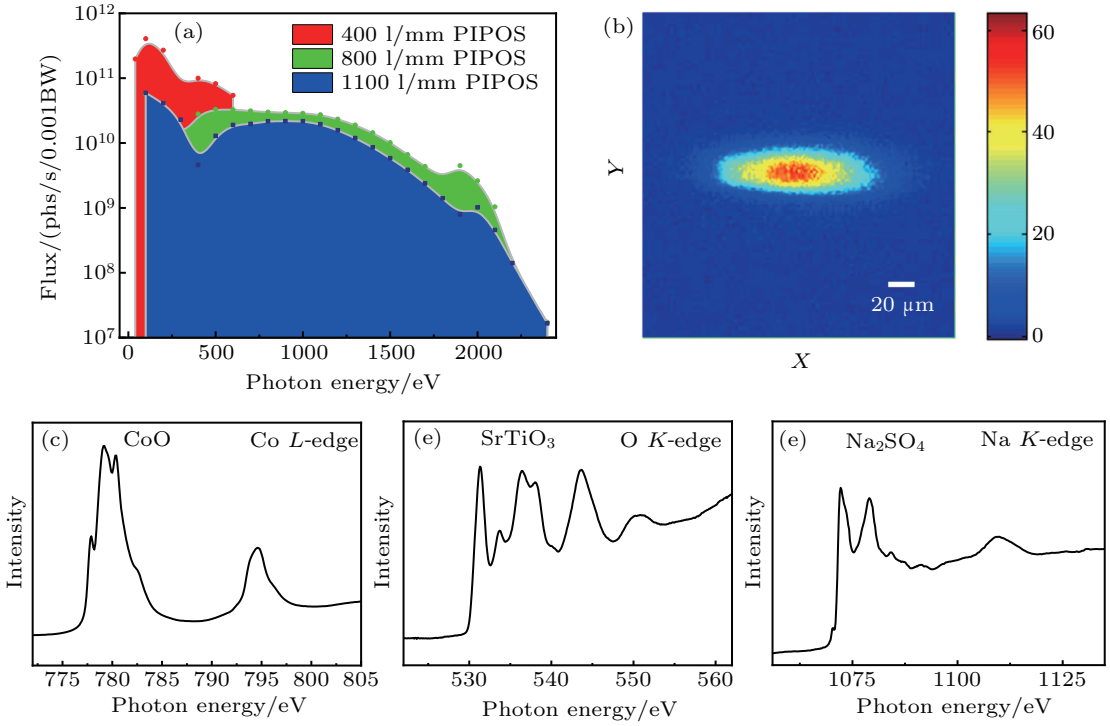


Fig. 5. (a) Photon flux at the PIPO endstation as a function of energy for different gratings.[23] (b) Spot size on PIPO sample, which is 150 μm×46 μm.[23] The high-resolution absorption spectra of (c) Co *L*-edge of CoO, (d) O *K*-edge of $SrTiO_3$, and (e) Na *K*-edge of Na_2SO_4.

Figure 6(a) shows the user's results on studying catalytic materials $Li_2Co_2O_4$ using sXAS at PIPO endstation.[17] By comparing with the reference sample, the *ex situ* Co *L*-edge XAS spectrum reveals that the content of Co^{4+} ions increases along with the *CV* cycles changing, which gives important information on the study of the catalytic mechanism. In addition, decreasing the jitter of the background currents helps us decrease the minimum amount of elements that can be detected in TEY mode. This feature is very important in studying surface catalysis, especially in the single-atom catalysis.

Comparing with TEY measurement, the TFY signal is much more dependent on the photon flux because the fluorescence yield is only about 1% while the electron yield is 99% in the soft x-ray region. When the sample is measured by TEY and TFY modes simultaneously, a balance between the resolution and signal to noise ratio of the spectrum needs to be achieved. We have optimized the distance between the TFY detector and the sample to 4 cm and slightly extended the scan time to 3 s/point to get a smooth TFY spectrum. The O *K*-edge TEY and TFY spectra of $Li_7La_3Zr_2O_{12}$ (LLZO) measured at PIPO endstation are shown in Fig. 6(b), a high-resolution and good signal to noise ratio have been achieved. LLZO is a promising solid electrolyte for lithium metal battery and Li_2CO_3 is formed on the surface when LLZO pellets are exposed to air.[29] By using the different detection depths of TEY ($\sim$ 10 nm) and TFY ($\sim$ 100 nm) modes, we can clearly verify the phenomenon. Only the signal of Li_2CO_3 can be observed in TEY spectrum while the signal of LLZO at 532 eV can be seen in TFY spectrum, which means the thickness of the Li_2CO_3 layer is slightly less than 100 nm. $SrTiO_3$ is the reference sample measured simultaneously for energy calibration.

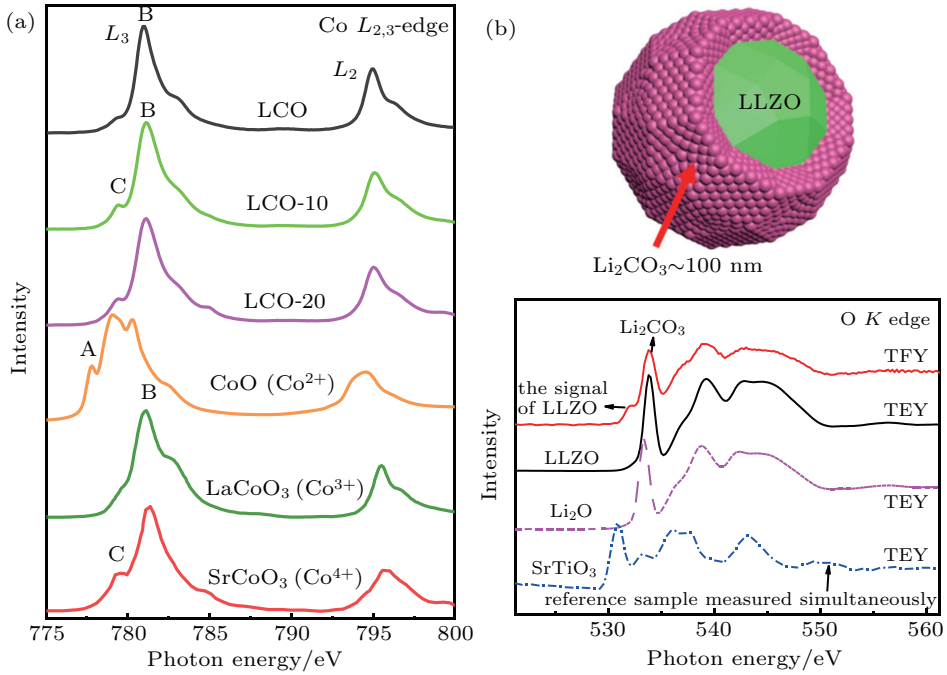


Fig. 6. (a) Co L-edge XAS spectra of $Li_2Co_2O_4$ samples. LCO represents $Li_2Co_2O_4$ samples, LCO-10 represents the $Li_2Co_2O_4$ samples underwent 10 *CV* cycles, and LCO-20 represents the $Li_2Co_2O_4$ samples underwent 20 *CV* cycles.[17] The references CoO (high spin, Co^{2+}), $LaCoO_3$ (low spin, Co^{3+}), and $SrCoO_3$ (low spin, Co^{4+}) spectra are shown for comparison.[17] (b) The O K-edge XAS results measured in TEY and TFY modes of a solid electrolyte LLZO.

4. Conclusion

A new PIPO endstation has been designed and constructed at beamline 02B02 of SSRF for the studies of energy and catalytic materials. By special designs, the signals of the reference sample, gold mesh, TEY, and TFY can be measured simultaneously. In the TEY mode, the jitter of the background current can be decreased to lower than 0.01 pA, which ensures us to achieve a smooth spectrum with only 1 pA current on the sample. High-resolution spectra of Co L-edge and O K-edge have been measured. In the TFY mode, a self-designed TFY detector using Sjuts CEM and Femto collector can achieve good signals even at a photon flux of 1×10^{11} photons/s $@E/\Delta E = 3700$. The sample holder is designed big enough for a series of samples and *in situ* tests of the coin cell. A special glove box is attached to the load-lock chamber for the air-sensitive samples. The preparation chamber is used for preprocessing the sample by Ar ion etching and vacuum annealing before the XAS tests. The *in situ* gas and liquid cells are developed for the PIPO endstation to study the samples under realistic working conditions. Our endstation is also part of a new beamline project ME^2 (Materials for Energy and Environment beamline), which combines most of the soft x-ray *in situ* characterization techniques (XPS, XAS, and ARPES) with *in situ* material growth capability. This beamline project has finished and is now fully opened to users.

Acknowledgments

We are very grateful to help from Prof. Yong Han at Shanghai Tech University and Prof. Zhi Guo, Prof. Xiangyu Meng in Shanghai Synchrotron Radiation Facility.

References

[1] Etacheri V, Marom R, Elazari R, Salitra G and Aurbach D 2011 *Energ. Environ Sci.* **4** 3243
[2] Cheng X B, Zhang R, Zhao C Z and Zhang Q 2017 *Chem. Rev.* **117** 10403
[3] Mefford J T, Rong X, Abakumov A M, Hardin W G, Dai S, Kolpak A M, Johnston K P and Stevenson K J 2016 *Nat. Commun.* **7** 11053
[4] Sun M H, Huang S Z, Chen L H, Li Y, Yang X Y, Yuan Z Y and Su B L 2016 *Chem. Soc. Rev.* **45** 3479
[5] Yu H S, Wei X J, Li J, Gu S Q, Zhang S, Wang L H, Ma J Y, Li L N, Gao Q, Si R, Sun F F, Wang Y, Song F, Xu H J, Yu X H, Zou Y, Wang J Q, Jiang Z and Huang Y Y 2015 *Nucl. Sci. Tech.* **26** 050102
[6] Cai J, Dong Q, Han Y, Mao B H, Zhang H, Karlsson P G, Åhlund J, Tai R Z, Yu Y and Liu Z 2019 *Nucl. Sci. Tech.* **30** 81
[7] Zheng L and Wu X S 2013 *Chin. Phys. B* **22** 107806
[8] Long X H, Wu Y R, Zhang N, Yu P F, Feng X F, Zheng S, Fu J M, Liu X S, Liu N, Wang M, Xu L M, Chen J M and Lee J M 2018 *Chin. Phys. B* **27** 107802
[9] Zhang N, Long X H, Wang Z, Yu P F, Han F D, Fu J M, Ren G X, Wu Y R, Zheng S, Huang W C, Wang C S, Li H and Liu X S 2018 *ACS Appl. Energy Mater.* **1** 5968
[10] Moses A W, Flores H G G, Kim J G and Langell M A 2007 *Appl. Surf. Sci.* **253** 4782
[11] Qiao R M, Wray L A, Kim J H, Pieczonka N P W, Harris S J and Yang W L 2015 *J. Phys. Chem. C* **119** 27228
[12] Wan G, Yu P F, Chen H R, Wen J G, Sun C J, Zhou H, Zhang N, Li Q R, Zhao W P, Xie B, Li T and Shi J L 2018 *Small* **14** e1704319
[13] Fu J M, Yu P F, Zhang N, Ren G X, Zheng S, Huang W C, Long X H, Li H and Liu X S 2019 *Energ. Environ Sci.* **12** 1404
[14] Qiao R M, Lucas I T, Karim A, Syzdek J, Liu X S, Chen W, Persson K, Kostecki R and Yang W L 2014 *Adv. Mater. Interfaces* **1** 1300115
[15] Liu X S, Wang D D, Liu G, Srinivasan V, Liu Z, Hussain Z and Yang W L 2013 *Nat. Commun.* **4** 2568

[16] Rao F, Song Z T, Cheng Y, Liu X S, Xia M J, Li W, Ding K Y, Feng X F, Zhu M and Feng S L 2015 *Nat. Commun.* **6** 10040
[17] Zhang S, Gu S Q, Wang Y, Liang C, Yu Y, Han L, Zheng S, Zhang N, Liu X S, Zhou J and Li J 2019 *ACS Catal* **9** 7389
[18] Yang J, Qiu Z Y, Zhao C M, Wei W C, Chen W X, Li Z J, Qu Y T, Dong J C, Luo J, Li Z Y and Wu Y E 2018 *Angew. Chem. Int. Ed. Engl.* **57** 14095
[19] Wan J W, Chen W X, Jia C Y, Zheng L R, Dong J C, Zheng X S, Wang Y, Yan W S, Chen C, Peng Q, Wang D S and Li Y D 2018 *Adv. Mater.* **30** 1705369
[20] Yu M J, Wang Y and Xu W 2016 *Chin. Phys. B* **25** 048701
[21] Yang J, Zhu F, Zhang Q, Wu Y, Wu X, Qin S, Dong J C and Chen D L 2013 *Chin. Phys. Lett.* **30** 046101
[22] Yu P F, Cui Z H, Meng J W and Guo X X 2013 *Chin. Phys. Lett.* **30** 036102
[23] Meng X Y, Guo Z, Wang Y, Zhang H, Han Y, Zhao G F, Liu Z and Tai R Z 2019 *J. Synchrotron Radiat* **26** 543
[24] Guo Z, Meng X Y, Wang Y, Liu H G, Zhang X Z, Li Z L, Xue L and Tai R Z 2017 *J. Synchrotron Radiat* **24** 877
[25] Guo J H, Luo Y, Augustsson A, Rubensson J E, Sathe C, Agren H, Siegbahn H and Nordgren J 2002 *Phys. Rev. Lett.* **89** 137402
[26] Guo J H 2013 *J. Electron. Spectrosc. Relat. Phenom.* **188** 71
[27] Arthur T S, Glans P A, Matsui M, Zhang R G, Ma B W and Guo J H 2012 *Electrochem. Commun.* **24** 43
[28] Liu X S, Liu J, Qiao R M, Yu Y, Li H, Suo L M, Hu Y S, Chuang Y D, Shu G J, Chou F C, Weng T C, Nordlund D, Sokaras D, Wang Y J, Lin H, Barbiellini B, Bansil A, Song X Y, Liu Z, Yan S S, Liu G, Qiao S, Richardson T J, Prendergast D, Hussain Z, de Groot F M F and Yang W L 2012 *J. Am. Chem. Soc.* **134** 13708
[29] Cheng L, Crumlin E J, Chen W, Qiao R M, Hou H M, Franz Lux S, Zorba V, Russo R, Kostecki R, Liu Z, Persson K, Yang W L, Cabana J, Richardson T, Chen G Y and Doeff M 2014 *Phys. Chem. Chem. Phys.* **16** 18294